Synthesis and biological evaluation of titanium dioxide/thiopolyurethane composite: anticancer and antibacterial effects

Rana R. El Sadda[1*] , Mai S. Eissa[1], Rokaya K. Elafndi[1], Elhossein A. Moawed[1], Mohamed M. El-Zahed[2] and Hoda R. Saad[3]

Abstract

Nanocomposites incorporating titanium dioxide (TiO_2) have a significant potential for various industrial and medical applications. These nanocomposites exhibit selectivity as antimicrobial and anticancer agents. Antimicrobial activity is crucial for medical uses, including applications in food processing, packaging, and surgical instruments. Additionally, these nanocomposites exhibit selectivity as anticancer agents. A stable nanocomposite as a new anticancer and antibacterial chemical was prepared by coupling titanium dioxide nanoparticles with a polyurethane foam matrix through the thiourea group. The titanium dioxide/thiopolyurethane nanocomposite (TPU/TiO_2) was synthesized from low-cost Ilmenite ore and commercial polyurethane foam. EDX analysis was used to determine the elemental composition of the titanium dioxide (TiO_2) matrix. TiO_2NPs were synthesized and were characterized using TEM, XRD, IR, and UV–Vis spectra. TiO_2NPs and TPU foam formed a novel composite. The MTT assay assessed Cisplatin and HepG-2 and MCF-7 cytotoxicity in vitro. Its IC_{50} values for HepG-2 and MCF-7 were 122.99 ± 4.07 and 201.86 ± 6.82 µg/mL, respectively. The TPU/TiO_2 exhibits concentration-dependent cytotoxicity against MCF-7 and HepG-2 cells in vitro. The selective index was measured against both cell lines; it showed its safety against healthy cells. Agar well-diffusion exhibited good inhibition zones against *Escherichia coli* (12 mm), *Bacillus cereus* (10 mm), and *Aspergillus niger* (19 mm). TEM of TPU/TiO_2-treated bacteria showed ultrastructure changes, including plasma membrane detachment from the cell wall, which caused lysis and bacterial death. TPU/TiO_2 can treat cancer and inhibit microbes in dentures and other items. Also, TPU/TiO_2 inhibits *E. coli*, *B. cereus,* and *A. niger* microbial strains.

Keywords Titanium dioxide, Thiourea, Polyurethane foam, Ilmenite ore, MCF-7, HepG-2, Selective index

Introduction

Ilmenite ($FeTiO_3$) is one of the most prevalent minerals and is the source of titanium dioxide (TiO_2) [1]. It is found in the different locations of the Egyptian Eastern Desert e.g., Abu Ghalaga, Korab kanci Hamra Dome, Kolmnab Abu Dahr, Um Effein, Wadi Rahaba, Um Ginud, and Wadi El Miyah (G. El Rokham) [2–4]. There are present between 24°15″ and 24°25″ N and 35°02″ and 35°06″ E (Fig. 1). Mineralization generates bands or lenses of massive ore intercalated with gabbro layers or disseminations gradational between massive ore bands and enclosing gabbro. The main ilmenite band extends

*Correspondence:
Rana R. El Sadda
rana.elsadda2018@gmail.com
[1] Chemistry Department, Faculty of Science, Damietta University, P.O. Box 34517, New Damietta, Egypt
[2] Botany and Microbiology Department, Faculty of Science, Damietta University, New Damietta, Egypt
[3] Geology Department, Faulty of Science, Damietta University, New Damietta, Egypt

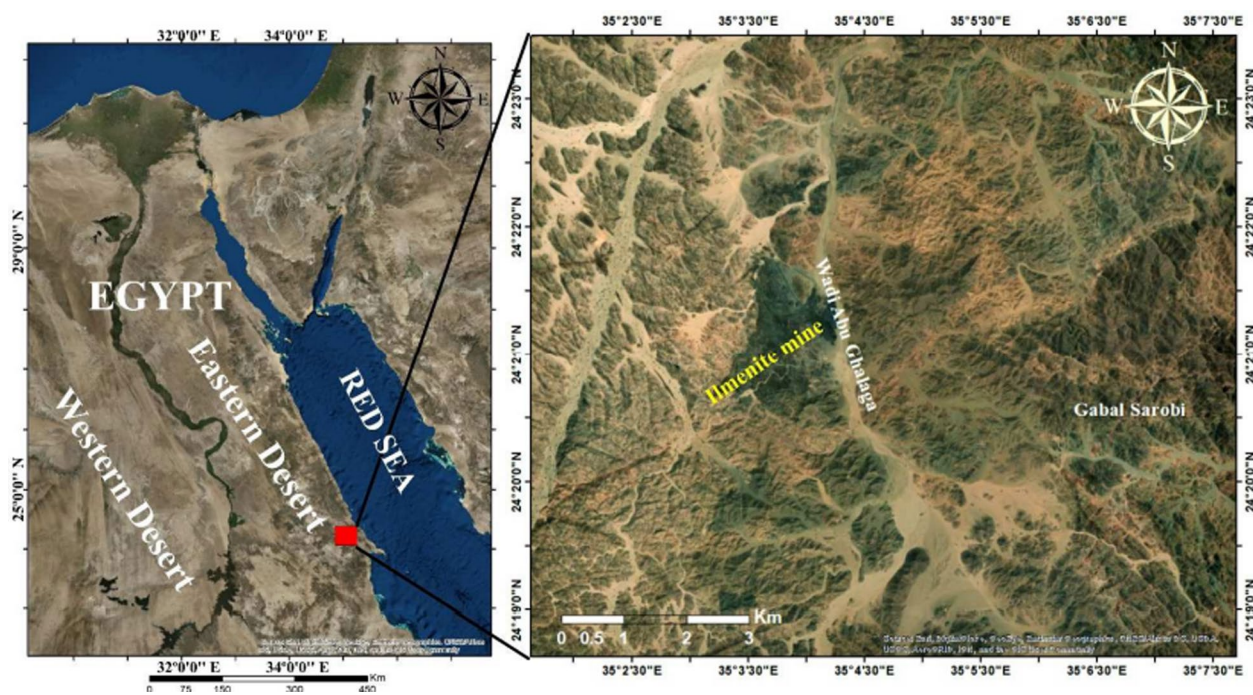El Sadda *et al. BMC Chemistry*   (2024) 18:35

Page 2 of 17

Fig. 1 Location Map of Wadi Abu Ghalaga

350 m in the northwest-southwest with 50 m wide and dips 45° to the northeast. The huge ore contains 70% ilmenite, magnetite, hematite, rutile, goethite, anatase, 28% silica minerals, and 3% sulfides [5, 6].

Titanium dioxide's antibacterial properties make its use in the food sector appealing. Where, food, pharmaceuticals, and cosmetics include harmless TiO_2. Due to their physical, chemical, and antibacterial properties, metal oxide NPs such as TiO_2 NPs have raised concerns in recent years [7–10]. They are thermally stable and eco-friendly. Ilmenite is the principal raw material for TiO_2 manufacturing because of the strong demand and the increasing growth of the sunscreen, toothpaste, and cosmetics sectors [11].

Polyurethane foam (PUF) is the principal polymeric substance used in industry and medicine. PUF's chemical composition and comfort are replacing earlier polymers. PUF foam resists, strengthens, and stabilizes, reducing maintenance time and cost [12–14]. Food processing, packaging, and safe transit are PUF's key uses. Refrigerators, freezers, food dryers, window frames, and furniture employ PUF for sound and cold insulation [15]. Nitrogen and sulfur give thiourea derivatives biological activity such as antibacterial, antifungal, anti-inflammatory, antioxidant, and anticancer [16, 17].

Cancer is a global killer. The WHO recommends finding new safe anticancer medicines [18]. Natural products can be exploited to generate anticancer medicines for lung, liver, breast, and pancreatic cancers [19]. Hepatocellular carcinoma (HCC) is the most frequent primary liver malignancy and the leading cancer killer worldwide [20–22]. Breast cancer kills most women worldwide, so it is necessary to focus on developing non-toxic anti-cancer medicines [18, 23].

Instead of limited chemotherapeutic treatments, stimuli-responsive delivery devices can provide tumor-targeted antitumor drugs. Drug delivery devices can reduce side effects, release, and damage to healthy tissue and organs [24]. systems (DDS) have been used to deliver therapeutic drugs for cancer treatment by either oral intake or injection [25]. Controlled drug delivery systems are improved to control the problems associated with conventional drug delivery [26]. Controlled drug delivery systems allow the drug to transport selectively to the target tissues, minimizing of its influence on vital tissues and undesirable side effects. Also, it protects the drug from rapid degradation and enhances drug concentration in target tissues, thus, lower drug doses are required [27].

In addressing the difficulties associated with conventional anticancer drugs and drug delivery systems (DDS), there is a pressing need for more focused and less side-effect-prone treatments. Researchers have explored various materials, including polymers, peptides, dendrimers, and hydrogels, as potential carriers for controlled release and targeted drug delivery. However, considerable challenges persist in the field of cancer treatment. A high

El Sadda *et al. BMC Chemistry*   (2024) 18:35

Page 3 of 17

molecular weight peptide, VPGVGVPGVG, was synthesized with sensitivity to temperature and pH. This peptide was employed as a carrier for the anticancer drug doxorubicin (Dox), and the conjugation was achieved through a hydrazone linkage. The specially designed peptide, the dual-sensitive peptide (DSP), demonstrated thermo-sensitive and pH-sensitive characteristics [28].

Injectable hydrogels, such as chitosan-based hydrogels, have shown potential for precise and non-invasive drug delivery [29]. Nucleic acid nanostructures have been engineered to respond to various stimuli, including pH, redox gradient, and light, for drug delivery applications [30]. Responsive delivery systems based on pH, light, and redox-cleavable polymers have been developed for controlled drug release [31]. Mesoporous silica nanoparticles (MSNs) with surface silanol groups have been utilized as versatile drug delivery platforms, with stimuli-responsive silanol conjugates enabling precise drug release [32]. Stimuli-responsive boron-based materials, such as boron nitride and boronic acid, have also been explored for controlled drug release in response to pH, light, and temperature [33]. These advancements in stimuli-responsive drug delivery systems have the potential to improve therapeutic efficacy and overcome the limitations of conventional drug delivery methods. Another study introduced the encapsulation of DHA-SBT-1214 in nanoemulsions to improve drug delivery. The properties and advantages of PEG-modified nanoemulsions, including enhanced blood circulation and efficient cellular uptake indicate that DHA-SBT-1214 delivered in nanoemulsions exhibits superior therapeutic efficacy against PPT2 cells and tumors, demonstrating potential as a novel CSC-targeted anticancer drug candidate with good tolerability in mice [34].

As a cutting-edge drug delivery technique, nanocarriers play a significant role in cancer treatment [9]. Nanoparticles, with their selective targeting capabilities and superior efficacy, have gained attraction in the field of medicine [35]. Their small size facilitates penetration through blood vessels and reduces non-specific binding, which improves their activity as a drug carrier [36]. Various targeting molecules can be conjugated on the surface of nanoparticles, which is an important aspect of drug delivery [9].

PUF, with its high surface area and biodegradation, can be used as a good substrate for cell attachment and drug delivery [37]. As an interesting substitute for conventionally utilized biodegradable polyesters, polyurethane can be employed to construct nano-carriers. Polyurethane foam is a promising choice as a targeted delivery system and a drug carrier. Polyester/ether urethanes (PURs) can replace biodegradable polyesters in nanocarriers. PURs can easily alter hydrophilic/hydrophobic equilibrium and have specific capabilities, making them a viable tailored delivery system [38].

The utilization of polymer-based micro- and nanoparticles in drug delivery systems offers distinct advantages, allowing for site-specific drug distribution within the body through cell-specific targeting. This approach provides better control over drug release kinetics [39]. Nanostructured polymers, formed by encapsulating antibiotic-loaded nanoparticles in carboxylated polyurethane, demonstrated controlled drug elution, extending antimicrobial activity for up to 8 days [40]. Alteration of the hard- and soft-segmented microstructure of polyurethane by incorporating polyester into the chain and introducing nanoparticles of polyurethane into polycaprolactone (PCL) as a carrier. This modification resulted in faster degradation, higher encapsulation efficiency, and a longer, more controlled drug release profile [41]. Coating composite shell scaffolds with gelatin-containing drug-loaded polyurethane nanoparticles is another method for maintaining scaffold microarchitecture and achieving sustained drug release [42]. Introduced a novel polyurethane nano micelle for multifunctional drug delivery with tumor-specific targeting and cleavage capabilities; this tumor-specific targeting ensures precision in drug delivery, while its cleavage capabilities offer a controlled release mechanism, potentially enhancing the therapeutic outcome while minimizing side effects [43]. Polyurethane–polyurea nanoparticles with adjusted hydrophobic and hydrophilic chains are used for drug delivery to achieve sub-30 nm nanoparticles, suggesting improved encapsulation stability compared to single-walled nanostructures [44].

Viruses, bacteria, and fungi cause most foodborne illnesses. Foodborne illnesses cause diarrhea, stomach cramps, nausea, vomiting, and fever [45, 46]. *Bacillus cereus* and *Escherichia coli* are common environmental pathogens that contaminate food. *B. cereus* is a gram-positive, motile, spore-forming bacterium, that germinates, thrives even after heat treatments, and creates enterotoxins that cause food poisoning [47]. *E. coli* is a gram-negative bacterium, which identifies fecal contamination and causes serious infections when consumed in contaminated foods. The Common food contaminant *Aspergillus niger* generates mycotoxins and aflatoxins. It also produces spores that cause aspergillosis, a dangerous lung illness [48, 49].

This work describes the TPU/TiO$_2$ nanocomposite synthesis. Thiourea and TiO$_2$ NP were added to PUF to increase its antibacterial, antifungal, and anticancer properties. MTT colorimetric assays assess cell viability and cytotoxicity. HepG-2 and MCF-7 cells model liver and breast cancer, respectively. *E. coli*, *B. cereus*, and *A.*

El Sadda *et al. BMC Chemistry*   (2024) 18:35

Page 4 of 17

niger were tested for TPU/TiO$_2$ antibacterial properties as models for bacterial and fungal diseases.

Materials and methods

Materials

TPU/TiO$_2$: The ilmenite ore was obtained from the Abu Ghalaga mine, an established mining operation at the intersection of Wadi Abu Ghusun and Wadi Abu Ghalaga in the southern Eastern Desert, and identified at the field (Fig. 2A and B). The Abu Ghalaga deposit occurs on a hill overlooking Wadi Abu Galaga, 20 km west of the port of Abu Ghosun. It lies between latitudes 24°15″ and 24°25″N and longitudes 35°02″ and 35°06″E. The fresh black ore samples were pulverized to -200 mesh.

Foamex Company (Damietta, Egypt) supplied commercial open-cell flexible PUF sheets (d = 12 kg/m^3) for foam manufacture, and sliced PUF sheets were 0.125 cm^3 cubic. Sigma-Aldrich and Adwic (Egypt) supplied all experiment chemicals (NH$_4$SCN, HCl, NaOH, NaHCO$_3$, Na$_2$CO$_3$, benzaldehyde, ethanol 70%, methanol, acetone, and benzene).

MCF-7 and HepG-2 cells were obtained from the American Type Culture Collection (ATCC) (Rockville, MD, USA). Sigma (USA) supplied MTT, trypan blue dye, and DMSO. Lonza (Belgium) supplied fetal bovine serum, RPMI-1640, HEPES buffer, L-glutamine, gentamycin, and 0.25% trypsin–EDTA.

ATCC bacterial strains like *E. coli* (ATCC 25922) and *B. cereus* (ATCC 6633) as well as the fungal strain of *A. niger* (van Tieghem 1867) from Microbiology Laboratory, Faculty of Science, Damietta University. Bacteria and fungi were sub-cultured on nutrient broth, and Dox agar (Oxoid, UK), respectively. Pfizer Co., Ltd. supplied penicillin G and fluconazole and Sigma (USA) supplied DMF.

Methods

The optimum conditions for the leaching of ilmenite ore and precipitated TiO$_2$ were studied. The effect of acid concentration (H$_2$SO$_4$ of 10–70%), time (14–90 min), temperature (50–250 °C), weight of ore (0.5–10 g) and acid volume (1–50 mL) were tested.

TiO$_2$NP: 25 g of ilmenite ore was cooked at 100 °C for 2 h in 60 mL of 30% H$_2$SO$_4$. After cooling, it was filtrated and rinsed 3 times with dist. H$_2$O. 250 mL dist. The filtrate was heated at 90 °C for 3 h with H$_2$O. The residue was filtrated, washed, dried overnight, and calcined at 800 °C for 2 h to yield TiO$_2$NP [50–52].

TPU: 10 g of PUF cubes were heated with stirring in 1 mol/L HCl for 3 h and rinsed well with distilled water. PUF cubes were washed in 50 mL of concentrated HCl and then 25 mL of 5 g/l NH$_4$SCN was added [53].

TPU/TiO$_2$: 4 g TPU and 2 g TiO$_2$ were refluxed in 200 mL ethanol at 60 °C for 2 h. TPU/TiO$_2$ was rinsed with distilled water, and ethanol, then it was air-dried.

Characterization

The infrared (IR) spectra were carried out using a KBr disc (KBr pellet) on a JASCO FTIR-410 spectrometer (Germany) in the 4000–400 cm^{-1} region. UV/VIS JASCO Spectrometer V-630 (Japan) was used for absorbance
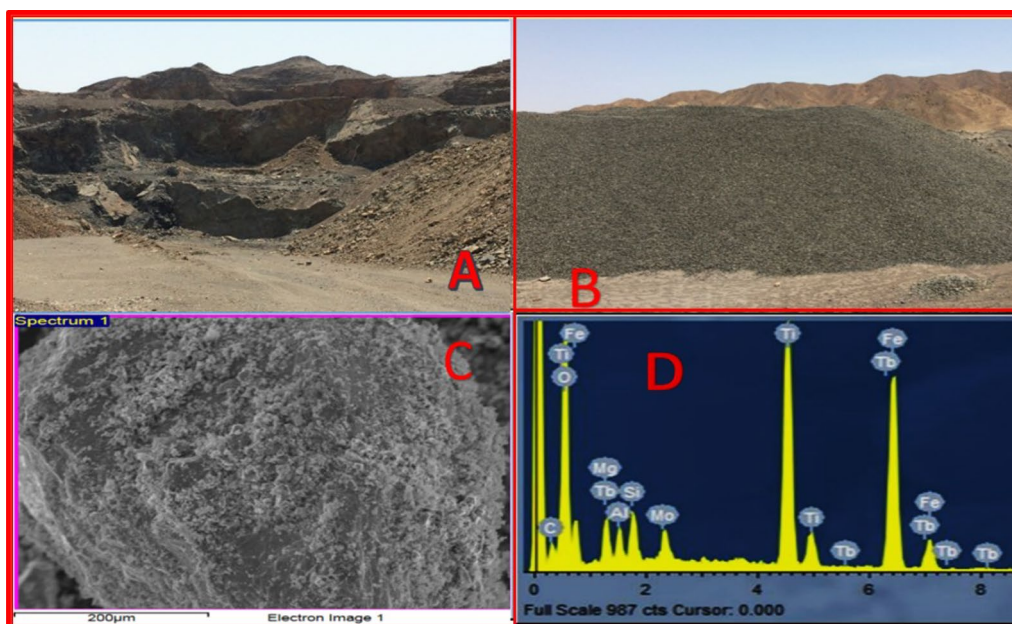

Fig. 2 **A** Surficial oxidized ore, **B** Crushed ilmenite ore, **C** SEM image of ilmenite ore at 200×magnification (**C**) and (**D**) EDX of ilmenite ore

El Sadda *et al. BMC Chemistry*   (2024) 18:35

Page 5 of 17

measurements. It measures the amount of light absorbed by a sample through a reference sample (water is the blank). MINIFLIX Benchtop Powder X-ray Diffractometer (USA) identified the crystalline phase. XRD data was performed in the faculty of sciences at Banha University. The morphological characteristics and elemental composition of the ilmenite sample were characterized using SEM and EDX (JEOL model JSM-6510LV, USA), at an accelerated voltage of 20 kV in the secondary electron mode. The fracture surface was vacuum-coated with gold and examined at 200 μm magnification. The size and morphology of the prepared TiO_2NPs were examined using a transmission electron microscope (TEM) Model Talos TM 120C, Thermo Fisher, Scientific, UK with an acceleration voltage of 120 kV. TEM was carried out in the Electron Microscope Unit at Damietta University. The ultrastructure study of treated bacteria was investigated using a JEOL JEM-2100, Japan, Electron microscope unit, Mansoura University operated at an accelerating voltage of 200 kV. The cells were cross-sectioned using an ultra-microtome, stained, and examined using TEM on carbon-coated copper grids (Type G 200, 3.05 μM diameter, TAAP, U.S.A.). Zeta potential of TPU/TiO_2 dispersion in water was conducted using Zetasizer, Malvern Instruments, Nano-ZS. It was measured three times at room temperature.

The acidic and basic sites of TPU/TiO_2 were determined using Boehm's titration. 0.5 gm of TPU/TiO_2 was added to 10 mL of 0.05 mol/L $NaHCO_3$, Na_2CO_3, NaOH, and HCl. After 24 h of soaking, the solutions were titrated against 0.05 mol/L HCl and NaOH. The total acidity (the sum of carboxyl, lactone, and phenolic groups) was recorded. The surface charge of TPU/TiO_2 was evaluated over the initial pH range of 2–14 and pH at the zero-charge point (pH_{PZC}) was determined. 0.5 gm of TPU/TiO_2 was added to 10 ml of each buffer solution and after 24 h, the final pH was also measured. The differences between the initial and final pH values were plotted against the initial pH. The chemical stability of TPU/TiO_2 was tested in different buffer solutions (pH: 2–14) and different organic solvents (e.g., CH_3OH, CH_3COCH_3, C_6H_6, C_6H_5CH3, DMF, and DMSO). 0.5 g of TPU/TiO_2 was soaked in 10 mL of each buffer solution and organic solvent for 24 h, then filtrated, dried, and weighted.

Anticancer activity

The Regional Centre for Mycology and Biotechnology (Al-Azhar University, Cairo) cultivated MCF-7 and HepG-2 cells. RPMI-1640 medium with 10% inactivated fetal calf serum and 50 μg/mL gentamycin supported cell growth. Cells were subcultured two to three times a week at 37 °C in a humidified environment with 5% CO_2.

Cytotoxicity: Colorimetric MTT assays assessed TPU/TiO_2's cytotoxicity on two cancer cell lines (breast-cancer cell line MCF-7 and hepatocellular carcinoma cell line HepG-2) cells in addition to healthy mammalian cells from African Green Monkey Kidney (Vero). MCF-7 and HepG-2 cells were suspended in media (5×10^4 cell/well) in 96-well tissue culture plates for 24 h. Twelve TPU/TiO_2 concentrations were introduced in three duplicates. Each 96-well plate had 6 vehicle controls with medium or 0.5% DMSO. The MTT test counted live cells after 24 h. Briefly, the media was withdrawn from the 96 well plates and replaced with 100 μL of fresh culture RPMI 1640 medium without phenol red, followed by 10 μL of the 12 mM MTT stock solution (5 mg MTT in 1 mL PBS) in each well, including the untreated controls. 96 well plates were incubated at 37 °C and 5% CO_2 for 4 h. An 85 μL aliquot of the medium was withdrawn from each well, and 50 μL of DMSO was added and mixed thoroughly with the pipette and incubated at 37 °C for 10 min [54, 55]. To count live cells, 590 nm optical density was assessed, calculating cell viability (Additional file 1). $Viability = (ODt/ODc) \times 100\%$ where OD_t is the mean optical density of TPU/TiO_2-treated cells and OD_c is that of untreated cells. The survival curve of each cancer cell line following TPU/TiO_2 treatment was plotted as a function of drug concentration and surviving cells. From graphic plots of the dose–response curve for each concentration, the 50% inhibitory concentration (IC_{50}) was determined by the following equation estimated the half-maximal effective concentration (EC_{50}) of TPU/TiO_2, which yields half-maximum response: $Y = Min + \frac{Max - Min}{1 + (\frac{X}{EC50})^{Hillcoefficient}}$

Antimicrobial action

Agar well-diffusion method: TPU/TiO_2's antimicrobial activity was tested against gram-negative *E. coli*; gram-positive *B. cereus*; *A. niger*. Clinical and Laboratory Standards Institute recommendations were followed for agar well-diffusion [56]. Nutrient and Dox agar were autoclaved (121 °C, 15 min) and coaled at 47 °C. Each 100 μL microbial culture ($1–2 \times 10^8$ CFU/mL) was injected into the agar media. Triplicate sterile Petri dishes were filled with inoculated agar material. After solidification, sterilized corkborers punctured 5-mm wells. TPU/TiO_2, Penicillin (antibacterial), and Fluconazole (antifungal) aliquots of 300 μg/mL in DMF were applied to the wells separately. Inoculated nutritional agar plates were incubated at 37 °C for 24 h and Dox agar plates at 30 °C for 5 days. After incubation, mm-sized inhibitory zones were detected.

Minimum inhibitory concentration (MIC): The TPU/TiO_2's MIC against gram-negative bacteria *E. coli* and

El Sadda *et al. BMC Chemistry*   (2024) 18:35

Page 6 of 17

gram-positive bacteria *B. cereus* was investigated [57]. Nutrient broth was made, autoclaved at 121 °C for 15 min, and coaled at 47 °C. In two sets of flasks, 100 μL of *E. coli* and *B. cereus* (0.5 McFarland standards ($1–2 \times 10^8$ CFU/mL)) were inoculated. Various quantities of sorbent (0–1000 μg/mL) were carefully put into each flask, with one serving as a positive control to monitor the normal development of the microbial cells in the absence of TPU/TiO_2. A negative control flask containing only cells and DMF was also made. For 24 h, the flasks were incubated in a shaker incubator (100 rpm) at 37 °C. Turbidity or cloudiness of the broth indicates the development of the inoculums in the broth, and the lowest concentration of TPU/TiO_2 that inhibited the growth of the test organism was chosen as the MIC. The optical density (OD) at 600 nm was measured spectrophotometrically to calculate the MIC value. The following formula was used to compute the growth inhibition percentage:

$$Growth\ inhibition\% = [(OD_C - OD_t)/OD_C] \times 100$$

where ODc and ODt are the OD of the control (without TPU/TiO_2) and tested TPU/TiO_2, respectively.

Minimum microbicidal concentration (MBC): Flasks of MIC for TPU/TiO_2 that had no apparent bacterial growth were inoculated into nutrient agar plates using the pour plate method and then incubated at 37 °C for 24 h. The MBC values of the antibacterial agents were determined with no apparent colonial bacterial growth plates El-Fallal [58].

Ultrastructural study: TPU/TiO_2 was tested on microbial ultrastructure using *E. coli.* Bacterial cell cultures were treated with TPU/TiO_2 for 2 h at 37 °C in nutritional broth. Bacteria were centrifuged at 5000 rpm for 15 min, and treated with 2.5% glutaraldehyde and 0.1 M cacodylate buffer, pH 7. TEM studied the ultrastructure of untreated and TPU/TiO_2-treated bacteria.

Data analysis: The mean ± standard deviation (S.D.) is the standard error of the mean. GraphPad Prism 6, San Diego, CA, estimated IC_{50}. Experimental data were analyzed using SPSS 19.0.

Results and discussion

Ilmenite and TiO_2 NP characterization

Ilmenite ore morphology and surface structure were examined using SEM at 200× magnification (Fig. 2C). The particle size of ilmenite was big and rough. EDX was performed to determine the elemental composition of ilmenite ore (Fig. 2D). The weight percentages of the principal components in the ilmenite matrix were carbon (9.5%), oxygen (39.3%), titanium (15.1%), iron (24.0%), terbium (4.7%), molybdenum (2.6%), magnesium (1.8%), silicon (1.7%), and aluminum (1.3%).

Tabassi et al. synthesized $TiFe_2O_4@Ag$ NPs which exhibited spherical shapes with a size range of 20–60 nm, and excellent stability (zeta potential of -47.7 mV). Anticancer evaluations demonstrated significant toxicity of $TiFe_2O_4@Ag$ NPs toward AGS gastric cancer cells ($IC_{50}=69.6$ μg/mL) compared to normal HEK293 cells ($IC_{50}=130$ μg/mL) through the MTT assay. This study introduces $TiFe_2O_4@Ag$ NPs as a novel and promising anticancer agent, emphasizing the need for further characterization for potential biomedical applications [59]. In another study by Cobos et al., they synthesized silver nanoparticles that were incorporated AgNPs into polymer matrices, such as polyvinyl alcohol (PVA) or chitosan, to create nanocomposites with enhanced antibacterial activity. These nanocomposites have shown effectiveness against various bacterial strains. Additionally, they can be functionalized with anticancer drugs for combined antibacterial and anticancer applications [60].

FTIR identified the ilmenite ore's functional groups (Fig. 3). OH group stretching caused ilmenite's 3388 cm^{-1} absorption band. Carbon dioxide O=C=O stretching caused 2347 cm^{-1} bands. OH bending bands are at 1598 cm^{-1}. The Ti–O matrix included 1086, 1009, 547, and 436 cm^{-1} peaks.

A UV–visible spectrophotometer at room temperature measured the ilmenite diffuse reflectance spectrum from 200–900 nm. The ilmenite sample strongly absorbs UV light at 234, 292, and 357 nm. Leaching mineral oxides from ilmenite ore with 30% H_2SO_4, precipitating with water, and calcining at 800 °C yielded TiO_2 NP. The FTIR spectra of TiO_2NP showed that the three stretching peaks appeared at 3732, 3382, and 2344 cm^{-1} for OH, H_2O, and O=C=O groups (Fig. 3). These groups were due to the physically and chemically adsorbed on the surface of TiO_2NPs. The TiO_2NP skeleton is represented by 1450 cm^{-1} bands. The Ti–O and Ti–O–Ti matrix had strong peaks at 1128, 879, 617, and 521 cm^{-1}.

Due to its white color, TiO_2NP was utilized industrially as a white pigment in paper, ceramics, rubber, textiles, paints, inks, cosmetics, and food coloring. Figure 4A shows the dazzling white TiO_2NP from ilmenite ore. The weight percentages of the key elements in TiO_2NP naturally synthesized from the ilmenite ore sample were O (52.2%), Ti (23.4%), Fe (2.8%), C (17.6%), S (3.1%), and Zn (0.9%), which determined the EDX spectrum (Fig. 4B).

TEM images showed TiO_2NP form and size (Fig. 4C). Single-particle TiO_2NP has uneven diameters. TiO_2NP particles averaged 47.1 nm. This particle size matched the literature results.

The TiO_2NP electronic spectrum was 200–900 nm. TiO_2NP absorbed UV light at 304 and 349 nm. From reflectance spectra, the optical bandgap (Eg) of TiO_2NP
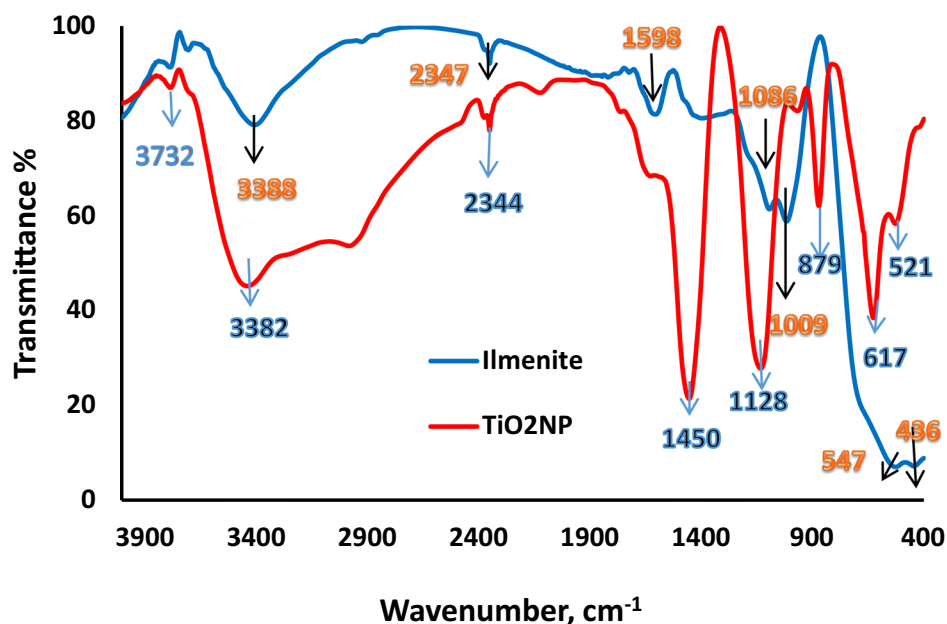
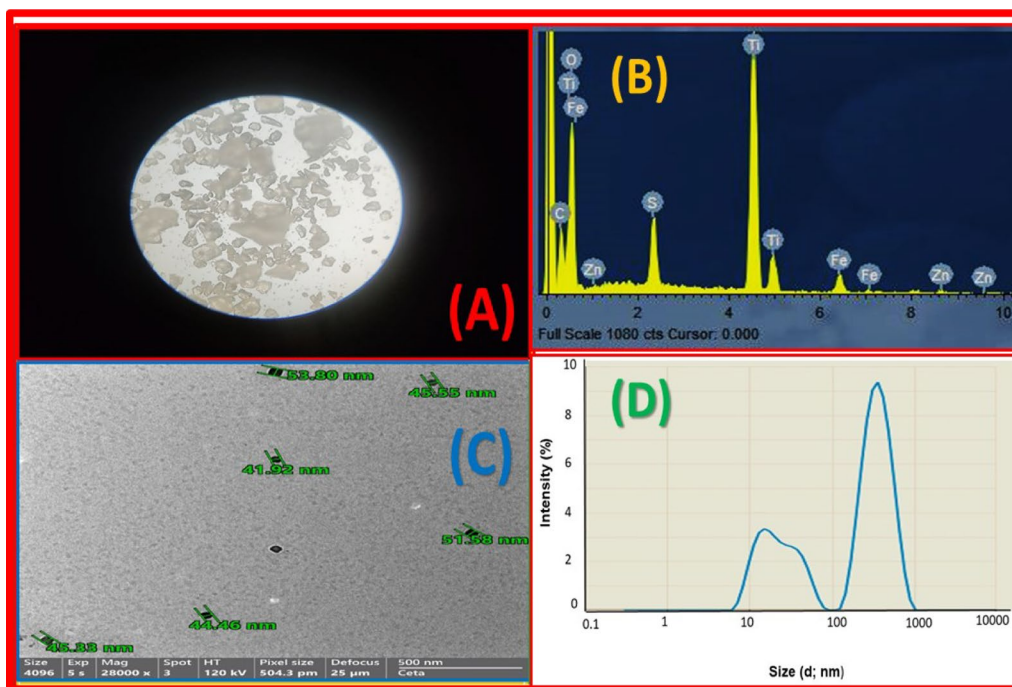**Fig. 3** FTIR spectra for ilmenite ore and titanium dioxide nanoparticles

Fig. 4 **A** White color image of TiO_2NPs, **B** EDX of TiO_2NPs **C** TEM of TiO_2NPs and **D** TiO_2NPs particles size distribution by Intensity

was calculated: where C is a constant, α is the absorption coefficient, A is the absorbance, and t is the thickness. The wavelength (nm) and energy h (eV) were computed.

The $(\alpha h)^2$ plotted versus h gives the energy gap at h = 0. TiO_2NP's direct band gap, semiconductor energy was 3.5 eV.

El Sadda *et al. BMC Chemistry* (2024) 18:35

Page 8 of 17

TPU/TiO$_2$ characterization

The particle size distribution of the TPU/TiO$_2$ nanocomposite varied from 41.58 to 63.94 nm (Fig. 4D). The mean diameter of the nanoparticles, according to DLS, was found to be 50.1 ± 12.09 nm.

FTIR spectroscopy identified TPU and TPU/TiO$_2$ functional groups (Fig. 5). In the FTIR spectrum of TPU, the characteristic peaks of TPU appeared at 2075 cm^{-1} (N=C=S), and 1540 cm^{-1} (N=C). Broadband from 3660 to 3272 cm^{-1} (−NH and −OH), several sharp peaks at 2910, 2867, 2857 cm^{-1} (−CH), 1668 cm^{-1} (C−O), 1639 cm^{-1} (C=C), and 1525 cm^{-1} (C−O−C) characterize the matrix of PUF. In the FTIR spectrum of TPU/TiO$_2$, TPU peaks were found at 3045, 2888, 2692, 2528, 1820, 1680, 2146, 2048, 1847, and 1076 cm^{-1}. Ti−O's characteristic band changed to 1296–545 and peaked at 487 cm^{-1}.

TPU and TPU/TiO$_2$ UV–Vis spectra were measured at 200–900. TPU substantially absorbed UV radiation at 350 nm in water, while TPU/TiO$_2$ absorbed it at 284 and 350 nm. For a straight band gap semiconductor, TPU and TPU/TiO$_2$ have 2.5 and 2.7 eV band gaps, respectively (Fig. 6). TPU/TiO$_2$'s greater particle size explains its lower energy gap (2.7 eV) than TiO$_2$NP's (3.5 eV). TPU/TiO$_2$ has higher surface polarity and electrical conductivity than TiO$_2$NP.

The TPU/TiO$_2$ and TPU magnetic susceptibility were determined using Evans balance data using the following equation: $\chi_g = CL(R - R_0)/10^9(M - M_o)$. Where: C is the balance calibration constant (1.35 cm), L is the sample height in cm, R is the balance reading for the sample in a tube, R$_o$ is the empty tube reading, M is the sample mass and tube in g, and M$_o$ is the empty tube mass in g.

TPU/TiO$_2$ has a low but positive magnetic susceptibility of 1.75×10^{-6} cm^3/mol. Paramagnetic TPU/TiO$_2$ was weakly magnetic. TPU has a diamagnetic magnetic susceptibility of 0.32×10^{-6} cm^3/mol.

The X-ray diffraction patterns of TPU/TiO$_2$ are shown in Fig. 7A and the peak details are in Table 1. The XRD patterns of TPU/TiO$_2$ showed a strong and narrow diffraction peak, which refers to the good crystallinity of the TPU/TiO$_2$ nanocomposite. The characteristic diffraction patterns of TPU/TiO$_2$ appeared at $2\Theta = 25.7$, 38.2, 48.4, 54.8, 62.9, 69.1, 70.7, 75.4 and 76.5; these correspond to crystal planes of (101), (004), (200), (105), (204), (116), (220), (215) and (301). The diffraction peaks at 25.7 (101), 38.2 (004), 48.4 (200), 54.8 (105), 62.9 (204), 70.7 (220) and 75.4° (215); were attributed to the anatase phase of TiO$_2$NPs. These patterns agree with the Joint Committee on Powder Diffraction Standards (JCPDS card no. 21-1272). However, the diffraction peaks at 2θ around 69.2 (116) and 76.5° (301); indicating the coupling between TPU and TiO$_2$NPs. The TPU/TiO$_2$ X-ray pattern exhibits a tetragonal crystal system (space group 141: I41/ amd:2). The order of their lattice parameters is as follows: (a=b=0.38 nm, c=0.95 nm and α=β=γ=90°). The results showed that modification of TPU with TiO$_2$NPs caused a phase change in the crystal structure. The particle size (D) of TPU/TiO$_2$ was calculated using the Debye–Scherrer equation ($D = 0.9\lambda/\beta cos\theta$). Where λ is the wavelength of X-ray (0.15418 nm), β is the peak
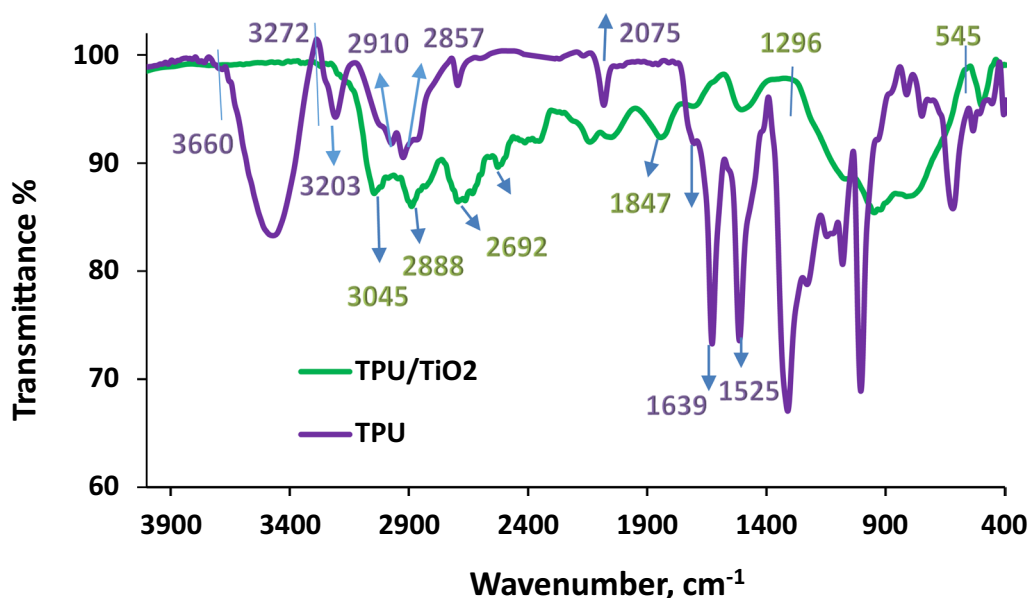

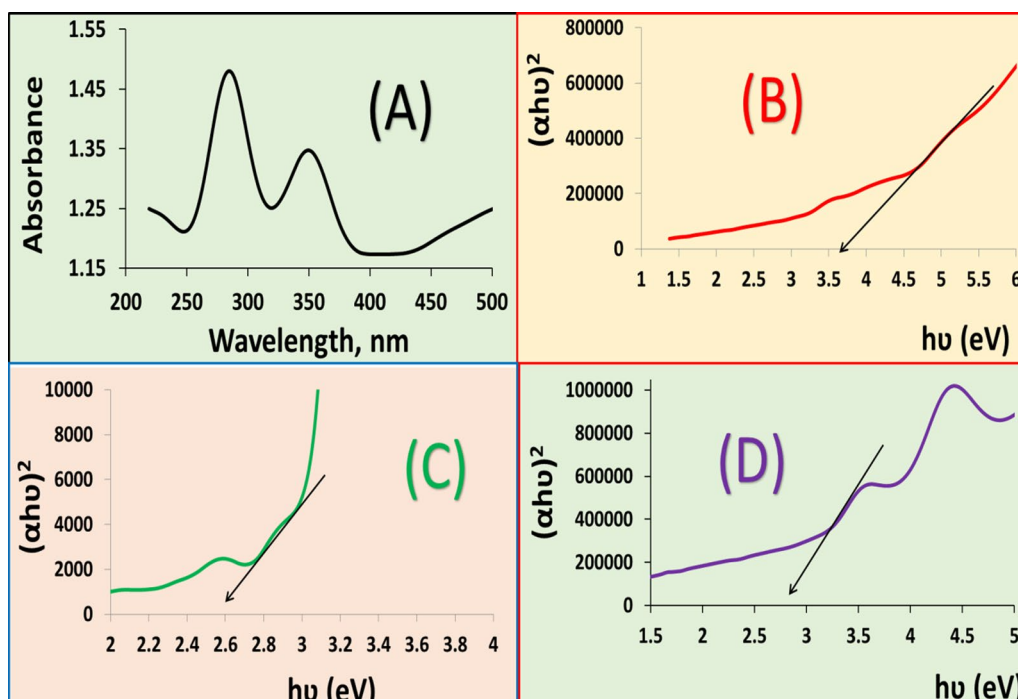**Fig. 5** FTIR spectra for TPU and TPU/TiO$_2$ nanocomposite

Fig. 6 **A** UV/Vis spectra for TPU/TiO$_2$, **B** band gap energy of TiO$_2$, **C** band gap energy of TPU and **D** band gap energy of TPU/TiO$_2$
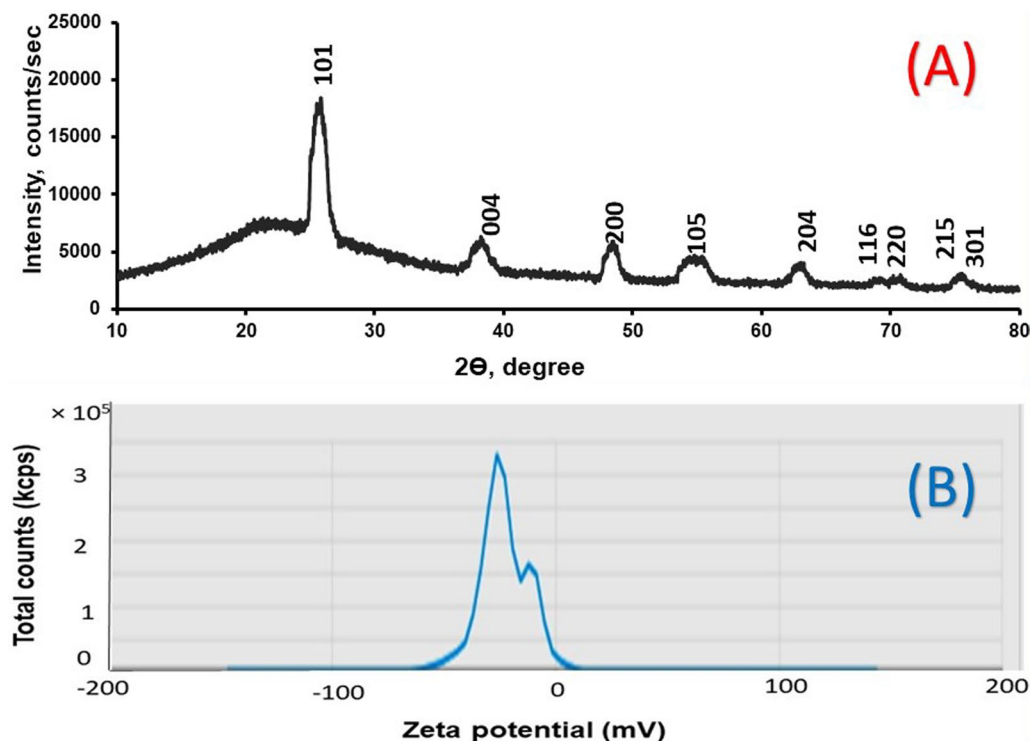

Fig. 7 **A** XRD patterns of TPU/TiO$_2$ nanocomposite and its corresponding Phase names **B** Zeta Potential Distribution of TPU/TiO$_2$

Table 1 XRD data for TPU/TiO$_2$

No.	2θ, °	Size, nm	FWHM, °	d, nm	Phase name
1	25.09881	18.797	0.4522	0.354516	Unknown
2	25.70177	8.68939	0.9794	0.346334	1 0 1
3	38.20488	5.6521	1.5536	0.235379	0 0 4
4	48.36408	8.40006	1.0828	0.188044	2 0 0
5	54.77334	4.6054	2.0291	0.167458	1 0 5
6	62.91277	8.41529	1.1558	0.147609	2 0 4
7	69.15261	10.36716	0.972	0.135734	1 1 6
8	70.70968	8.64852	1.1763	0.133122	2 2 0
9	75.42829	9.49174	1.105	0.125923	2 1 5
10	76.55398	33.14299	0.3189	0.124349	3 0 1

full width at half maximum (FWHM) in radians and θ is the Bragg diffraction angle. The average crystallite size of TPU/TiO$_2$ was in the range of 4.6–33.14 nm. Inter-planar spacing between atoms (d-spacing) is calculated using Bragg's Law: $2dsin\theta = n\lambda$.

Zeta potential analysis was performed to study the surface stability and charge of the nanoparticles. The zeta potential analysis revealed that the nanoparticles were stable with a zeta potential value of -22.85 ± 10.81mv Fig. 7B. It was stated that TPU/TiO$_2$ nanoparticles had negatively charged on their surface.

Boehm's titration determined TPU/TiO$_2$'s acidic and basic sites. TPU/TiO$_2$ had 60 mmol/g acidic sites and minimal basic sites. Over an initial pH range of 2–14, the surface charge and pH at zero charge point (pH$_{PZC}$) of TPU/TiO$_2$ were determined. TPU/TiO$_2$ has a pH$_{PZC}$ of 4. The TPU/TiO$_2$ surfaces are positively charged at pH < 4 and negatively charged at pH > 4. The chemical stability of TPU/TiO$_2$ was examined in several buffer solutions (pH 2–14) and organic solvents e.g., CH$_3$OH, CH$_3$COCH$_3$, C$_6$H$_6$, C$_6$H$_5$CH$_3$, DMF, and DMSO. TPU/TiO$_2$ weights were unaffected by testing solutions and solvents, after 24 h soaking, confirming their chemical stability.
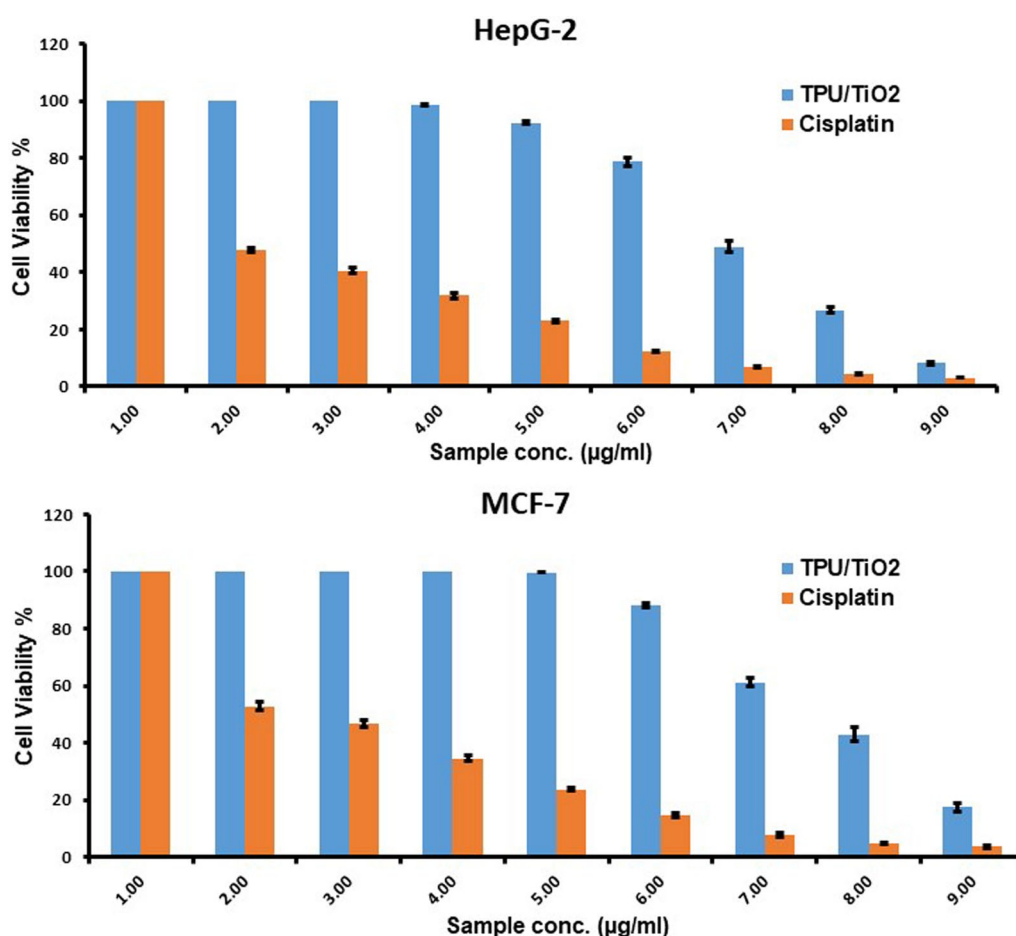

Fig. 8 **A** Cytotoxicity assessment of TPU/TiO$_2$ and Cisplatin (reference drug) against MCF-7 cells after 24 h of treatment **B** Cytotoxicity assessment of TPU/TiO$_2$ and Cisplatin (reference drug) against HepG-2 cells after 24 h of treatment

TPU/TiO$_2$ antitumor activity

TPU/TiO$_2$ was tested for cytotoxicity on MCF-7 and HepG-2 cells (Fig. 8). MCF-7 and HepG-2 cell viability curves were estimated after 24 h of treatment with TPU/TiO$_2$ (0–500 μg/mL). TPU/TiO$_2$ was cytotoxic to HepG-2 and MCF-7 cells with IC$_{50}$ values of 122.99±4.07 and 173.58±6.82 μg/mL respectively. Cisplatin IC$_{50}$ values for HepG-2 and MCF-7 cells were 3.58±0.34 and 5.72±0.59 μg/mL respectively (Table 2). TPU/TiO$_2$ has a

Table 2 IC$_{50}$ and selectivity index SI values of TPU/TiO$_2$ and Cisplatin in MCF-7 and HepG-2 cells (24 h treatment)

Cell line	IC$_{50}$ values ± SD (μg/ml) after 24 h			Selective index (SI) = IC50 (VERO) /IC50 (Carcinogenic cell line)	
	MCF-7	HepG-2	Vero	MCF-7	HepG-2
TPU/TiO$_2$	173.58±6.82	122.99±4.07	126.61±3.89	0.729	1.029
Cisplatin	5.72±0.59	3.58±0.34	2.06±1.58	0.360	0.575

MCF-7: Breast cancer cell line. HepG-2: Hepatocellular carcinoma. Vero: Mammalian cells from African Green Monkey Kidney.Selectivity index (SI) = [IC50 (vero)/IC50 (HePG2)]. The higher the SI ratio, the theoretically more effective and safer a drug

Table 3 EC$_{50}$ of TPU /TiO$_2$ and Cisplatin in MCF-7 and HepG-2 cells

Cell line	EC50	
	TPU/TiO$_2$	Cisplatin
MCF-7	173.59	6.31
HepG-2	127.34	4.81

lower IC$_{50}$ for HepG-2 than MCF-7, indicating that TPU/TiO$_2$ will work better for HepG-2 than MCF-7. Nanocomposite specifically reacts to the tumor microenvironment, enhancing drug accumulation in the tumor while reducing its side effects on non-cancerous tissues, which improves therapy. EC$_{50}$ for HepG-2 and Cisplatin were 127.34 and 4.81, respectively. Moreover, EC$_{50}$ for MCF-7 and cisplatin were 173.59 and 6.31 (Fig. 9 and Table 3). TPU/TiO$_2$ nanocomposite had greater IC$_{50}$ and EC$_{50}$ values than cisplatin. Toxicity, pharmacokinetics, and side effects should be considered when comparing drugs. A novel drug with a higher IC$_{50}$ and high selective index (SI) value may be as effective as cisplatin. The calculated SI ratios of TPU/TiO$_2$ for MCF-7 and HepG-2 were 0.729 and 1.029, respectively. While SI values of cisplatin for MCF-7 and HepG-2 were 0.360 and 0.575, respectively.
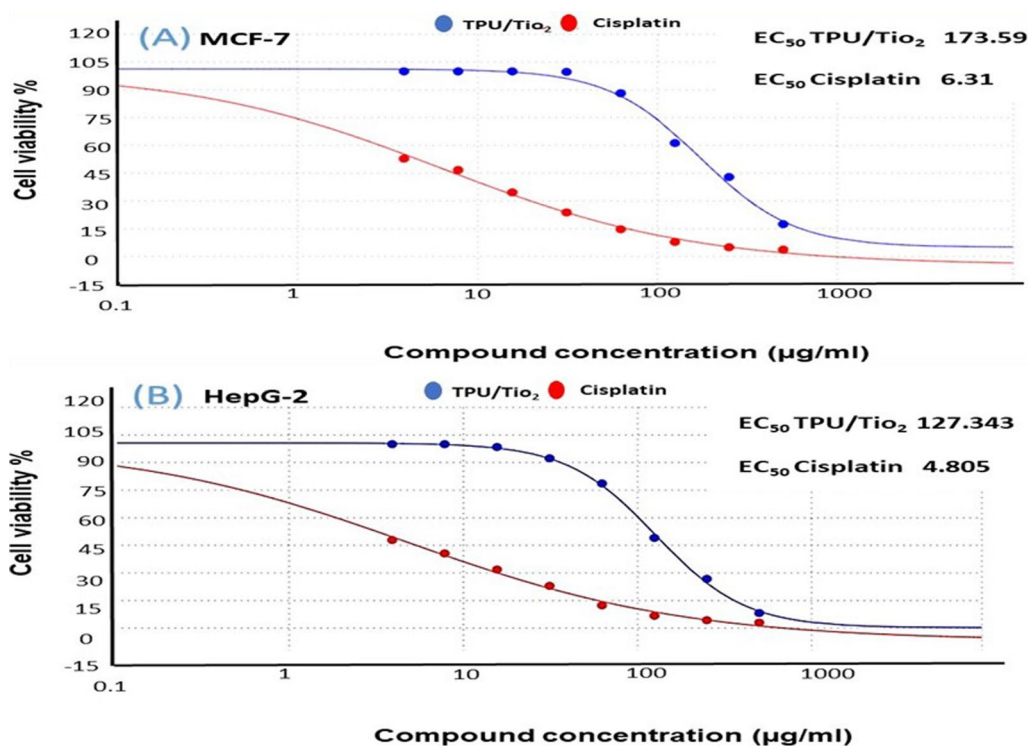

Fig. 9 Semi Log dose–response curves and calculated EC$_{50}$ values of TPU/TiO$_2$ (in blue) in comparison to Cisplatin (in red) against (**A**) MCF-7 (**B**) HepG-2 cells. Cell viability was determined using MTT assay
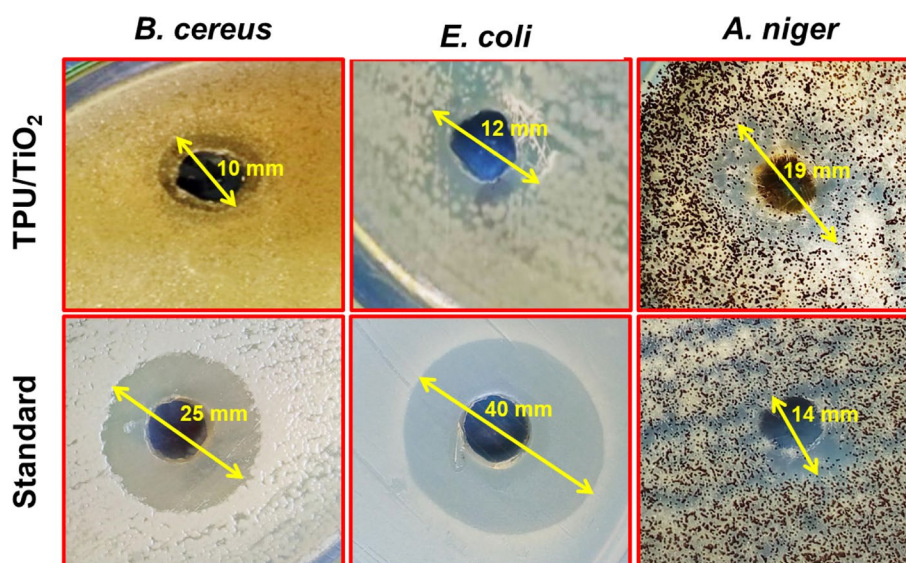
Fig. 10 Antimicrobial activity of TPU/TiO$_2$ in comparison with Penicillin (standard antibacterial) and Fluconazole (standard antifungal) using agar well diffusion method against *B. cereus*, *E. coli*, and *A. niger*. Arrows denote the diameter of inhibition zones (mm)

This is further evidence indicating that applying TPU/TiO$_2$, contrary to cisplatin, for treating cancer cell lines is expected to show minimal or no toxicity for healthy cells. Furthermore, TPU/TiO$_2$ shows more activity against HepG-2 than MCF-2. Our results agreed with those of Hassan et al., who used PdNPs and polyionic cross-linked chitosan (PICCS@Pd) nanocomposite as a nanocarrier for the delivery of doxorubicin (DOX) and 5-fluorouracil (5-FU) individually and in a cocktail. This new nanocomposite demonstrated excellent selectivity to attack tumor cells (MCF-7 and HT-29) compared to normal cells (HSFs) [61]. El Sadda et al. studied vitamin C and aspirin against the HepG-2 cell line; they showed higher selectivity than doxorubicin, which is referred to as standard therapy [62]. Also, similar to Payolla et al., vanadium-based compounds showed a greater selectivity index and better in vitro results than cisplatin [63].

Gambogic acid-TiO$_2$ nanocomposite caused photodynamic therapy (PDT)-induced apoptosis and necrosis in HepG-2 cells, according to another study. TiO$_2$ nanofibers can reduce drug intake in HepG-2 cells and prevent adverse effects on normal cells and tissue, which could be used in cancer treatment alliances. These nanocomposites modulate medication release [24]. Thiourea derivatives inhibited PTKs, topoisomerase II, human-type proteins, and DNA repair production, making them attractive anticancer treatments. Abbas et al. found that thiourea that used it as a structure modification selectively killed HepG-2 cancer cells over MCF-7 [64]. We should say that the incorporation of nano-sized carbon into the polyurethane matrix improved the antithrombogenicity of the polyurethane materials. It might be a novel and promising approach to developing biomaterials with high blood compatibility.

Antimicrobial TPU/TiO$_2$

While polyurethane foam (PUF) used for industrial and medical uses does not have to be antiseptic, antimicrobial activity is essential for medical indications such as food processing, packaging, and surgical instruments So, is PUF's antibacterial action related to any negative alterations in cell viability in vitro? To answer this question, we investigated the antimicrobial cytotoxic activity properties of a titanium dioxide/the polyurethane composite (TPU/TiO$_2$). TPU/TiO$_2$ represented low cytotoxic and high antimicrobial activities. In contrast, Cisplatin is known to have high cytotoxic and antimicrobial activity. Although PUF used for industrial and medical purposes does not have to be antimicrobial, the control of infection transmission from one person to another as well as the need for new effective agents against microbial resistance and low cytotoxic anticancer agents require antimicrobial activity.

Table 4 Antimicrobial effect of TPU/TiO$_2$ in comparison with Penicillin (standard antibacterial) and Fluconazole (standard antifungal)

Compound	Zones of inhibition (mm ± SD)		
	E. coli	*B. cereus*	*A. niger*
TPU/TiO$_2$	12 ± 0.06	10 ± 0.03	19 ± 0.14
Penicillin	40 ± 0	25 ± 0.03	–
Fluconazole	–	–	14 ± 0.14

El Sadda *et al. BMC Chemistry*   (2024) 18:35

Page 13 of 17

Agar well diffusion

TPU/TiO$_2$ inhibited *E. coli*, *B. cereus*, and *A. niger* using agar well diffusion. Figure 10 and Table 4 show that TPU/TiO$_2$ has good antibacterial action. TPU/TiO$_2$ inhibited gram-negative *E. coli* better. Gram-positive *B. cereus* with 12- and 10-mm inhibitory zones. Penicillin G outperformed TPU/TiO$_2$. The TPU/TiO$_2$ was more antifungal against *A. niger* than Fluconazole. Benzyl penicillin or penicillin G (the used antibiotic) generally has poor gram-negative activity, on the other hand, if it was dissolved in an organic solvent such as DMF which had synergistic effects, via damage to the bacterial membranes, that increased its potency by providing greater access to the periplasm/peptidoglycan. Literature value ranges for minimum inhibition concentration (MIC) of penicillin G against *E*. coli (ATCC 25922) were recorded as 16–64 µg/mL and inhibition zones ranged from 25–45 mm [65–70]. While Hossain et al. described *E. coli* (ATCC 25922) as an intermediate-resistant bacteria that had a MIC of penicillin G reaching 16 µg/mL [71]. TPU/TiO$_2$ was more antifungal against *A. niger* than Fluconazole. Acidic substances like peptidoglycan give microorganisms a negative charge. Gram-positive bacteria have higher cell wall negative charge values due to larger peptidoglycan coatings [72, 73]. TPU/TiO$_2$'s negative charge may repel germs, reducing its antibacterial efficacy compared to Penicillin G. Gram-positive bacteria (high peptidoglycan content) had a greater repulsion force than gram-negative bacteria, which may reduce their antibacterial activity.

Despite ROS production and membrane damage, TiO$_2$NPs may be effective antibacterial agents against microbial pathogens [74]. Thiourea is bound to peptides in the microbial cell wall, substantially down-regulating glucose, alanine, aspartic acid, glutamic acid, arginine, and proline metabolism. This action may kill enzymes that are crucial to microbial development [75]. Marzi et al. proposed thiourea derivatives as potent killers for *B. cereus* and *E. coli* that produced inhibition zones of 11 and 9 mm, respectively [76]. Thiourea compounds also inhibited *E. coli* with inhibition zones ranging from 14 to 23 mm according to [77]. Anbumani et al. also found that TiO$_2$ NPs kill *B. subtilis* (15 ± 0.46 mm), *E. coli* (35 ± 0.44 mm) *and A. niger (*21 ± 0.46 mm) [78].

MIC and MBC studies

The MIC of TPU/TiO$_2$ against *B. cereus* and *E. coli* was determined. MIC is defined in vitro as the lowest concentration of TPU/TiO$_2$ that causes complete inhibition of visible bacterial growth after incubation for 24 h. Figure 11 shows the growth inhibition curve of *E. coli* and *B. cereus* in the presence of different concentrations of TPU/TiO$_2$. The antibacterial ratios of TPU/TiO$_2$ MIC values against *B. cereus* and *E. coli* were 550 and 400 µg/mL, respectively. The MBC results were similar to MIC values which indicated the potent action of TPU/TiO$_2$ against the tested bacteria. Similarly, Abdulazeem et al. [79] documented the MIC and MBC values of TiO$_2$ against *E. coli* as 150 and 500 µg/mL, respectively. On the other Mahdy et al. reported that 40 µg/mL could inhibit *E. coli* growth
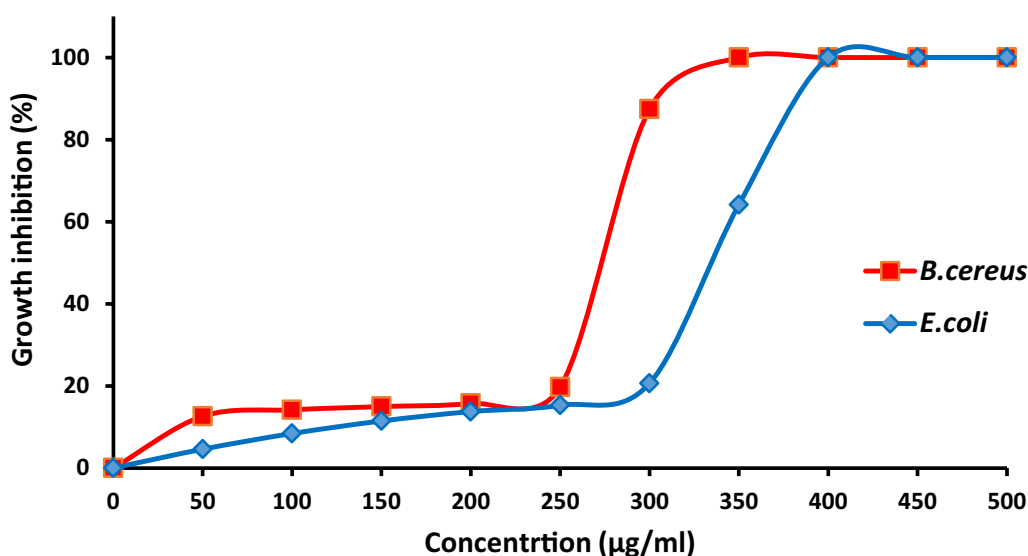

Fig. 11 Growth inhibition percentage of *E. coli* and *B. cereus* in the presence of different concentrations of TPU/TiO$_2$
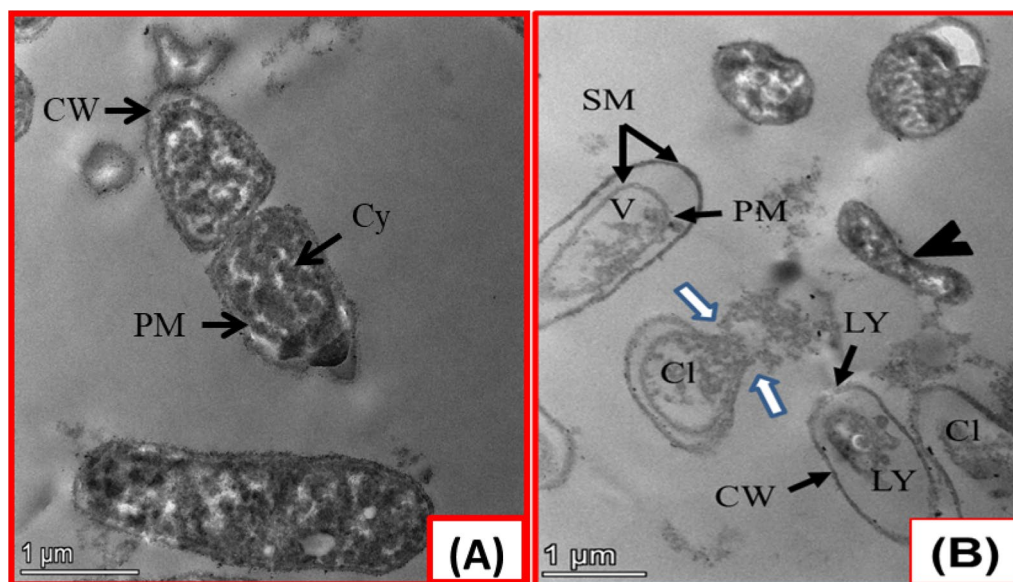
Fig. 12 The bactericidal effect of TPU/TiO$_2$ on the ultrastructure of *E. coli*. **a** A negative control (without TPU/TiO$_2$). **b** A treated sample, there are malformed irregular rods (black arrowhead) with lysed cell walls (LY), separation between cell wall and plasma membrane (SM), departure of cellular content from the cell (white arrows), vacuole formation (V), and a complete cell lysis (Cl). CW, PM, and Cy refer to cell wall, plasma membrane and cytoplasm, respectively

as strong MIC [80]. While Younis et al. recorded that the MIC of TiO$_2$ against *E. coli* reached 1500 μg/mL [81]

Ultrastructure research

TPU/TiO$_2$'s antibacterial mechanism is unknown; however, TiO$_2$NPs and thiourea may interact with microbial cell membranes and protein content to halt metabolic, respiratory, and cell division [82–84]. The ultrastructure morphology of untreated and TPU/TiO$_2$-treated *E. coli* bacteria is shown in Fig. 12. Untreated *E. coli* had full cell walls and rod-like forms. The cell walls of *E. coli* looked wrinkled, broken, and detached from the plasma membrane, releasing cellular material. TPU/TiO$_2$ also caused uneven rod deformity, vacuole development, and cell lysis. These studies suggest improving TPU/TiO$_2$ for industrial and biological applications.

Conclusion

We synthesized TiO$_2$ from low-cost Ilmenite ore from Abu Ghalaga, Egypt. TiO$_2$NPs and thiourea PUF formed TPU/TiO$_2$, a novel nanocomposite. TPU/TiO$_2$ was characterized using IR, UV–Vis, bandgap energy, magnetic susceptibility, chemical stability, and pH$_{PZC}$. TPU/TiO$_2$ inhibits *E. coli* and other microbial strains *e.g., B. cereus, A. niger.* TPU/TiO$_2$ exhibits concentration-dependent cytotoxicity against MCF-7 and HepG-2 cells in vitro. Studying in vivo applications is intriguing.

Abbreviations

EDX	Energy-dispersive X-ray spectrometry
MTT	Methyl thiazolyl diphenyl-tetrazolium bromide
HepG-2	Hepatocellular carcinoma cell line
MCF-7	Michigan Cancer Foundation-7 (breast cancer cell line)
TPU	Thiourea polyurethane
TiO$_2$NP	Titanium dioxide nanoparticles
PDT	Photodynamic treatment
PTKs	Protein tyrosine kinases
ROS	Reactive oxygen species
PUF	Polyurethane foam
OD	Optical density
HCC	Hepatocellular carcinoma
PURs	Polyester/ether urethanes
TEM	Transmission electron microscope
XRD	X-ray diffraction
IR	Infrared spectroscopy
IC$_{50}$	The 50% inhibitory concentration
ANS	Arabian–Nubian Shield
EC$_{50}$	The half-maximal effective concentration
S.D	Standard deviation
SI	Selective Index

Supplementary Information

The online version contains supplementary material available at https://doi.org/10.1186/s13065-024-01138-x.

Additional file 1: Table S1. Cytotoxicity effects of TPU/TiO$_2$ and Cisplatin (reference drug) against MCF-7 cells in vitro. **Table S2.** Cytotoxicity effects of TPU/TiO$_2$ and Cisplatin (reference drug) against HepG-2 cells in vitro.

El Sadda *et al. BMC Chemistry*   (2024) 18:35

Page 15 of 17

Data availability
The datasets used and/or analyzed during the current study are available from the corresponding author on reasonable request.

Declarations

Ethics approval and consent to participate
Not applicable.

Consent for publication
Not applicable.

Competing interests
The authors declare that they have no competing interests.

References

1. Mulyono JE, Soepriyanto S. Synthesis and characterization of TiO_2 from Ilmenite by caustic fusion process for photocatalytic application. AIP Conf. Proc. 2017;1805:030010. https://doi.org/10.1063/1.4974421.
2. El-Desoky HM, Abdel-Rahman AM, Fahmy W, Khalifa I, Mohamed SA, Shirazi A, Pour AB. Ore genesis of the Abu Ghalaga ferro-ilmenite ore associated with neoproterozoic massive-type gabbros, south-eastern desert of Egypt: evidence from texture and mineral chemistry. Minerals. 2023;13:307.
3. Khedr MZ, Takazawa E, Arai S, Stern RJ, Morishita T, El-Awady A. Styles of Fe–Ti–V ore deposits in the neoproterozoic layered mafic-ultramafic intrusions, south Eastern Desert of Egypt: evidence for fractional crystallization of V-rich melts. J Afr Earth Sc. 2022;194:104620.
4. Saleh GM, Khaleal FM, Lasheen ESR. Petrogenesis of ilmenite-bearing mafic intrusions: a case study of Abu Ghalaga area, South Eastern Desert, Egypt. Arab J Geosci. 2022;15:1508.
5. Basta EZ, Takla MA. Distribution of opaque minerals and the origin of the gabbroic rocks of Egypt. Bulletin of the Faculty of Science, Cairo University. 1974:347–364. https://api.semanticscholar.org/CorpusID:132323500.
6. Amin MS. The ilmenite deposit of Abu Ghalqa, Egypt. Econ Geol. 1954;49:77–87.
7. Chawla R, Sivakumar S, Kaur H. Antimicrobial edible films in food packaging: current scenario and recent nanotechnological advancements—a review. Carbohydr Polym Technol Appl. 2021;2:100024.
8. Chen X, Selloni A. Introduction: titanium dioxide (TiO_2) nanomaterials. Chem Rev. 2014;114:9281–2.
9. Khan I, Saeed K, Khan I. Nanoparticles: properties, applications, and toxicities. Arab J Chem. 2019;12:908–31.
10. Wu, X. Applications of Titanium Dioxide Materials. In Titanium Dioxide—Advances and Applications; IntechOpen: London, UK. 2022.
11. Turci F, Peira E, Corazzari I, Fenoglio I, Trotta M, Fubini B. The crystalline phase modulates the potency of nanometric TiO_2 to adhere to and perturb the stratum corneum of porcine skin under indoor light. Chem Res Toxicol. 2013;26:1579–90.
12. Howard GT. Biodegradation of polyurethane: a review. Int Biodeterior Biodegrad. 2002;49:245–325.
13. Sienkiewicz N, Członka S. Natural additives improve polyurethane antimicrobial activity. Polymers. 2022;14:2533.
14. Yang H, Yu B, Song P, Maluk C, Wang H. Surface-coating engineering for flame retardant flexible polyurethane foams: a critical review. Compos B Eng. 2019;176:107185.
15. Qiao M, Ren T, Huang TS, Weese J, Liu Y, Ren X, Farag R. N-Halamine modified thermoplastic polyurethane with rechargeable antimicrobial function for food contact surface. RSC Adv. 2017;7:1233–40.
16. El-Zahed MM, Kiwaan HA, Farhat AA, Moawed EA, El-Sonbati MA. Anti-candidal action of polyurethane foam: a new modifier with functionalized isothiouronium group. Iran Polym J. 2023;32:71–9.
17. Faihan AS, Hatshan MR, Kadhim MM, Alqahtani AS, Nasr FA, Saleh AM, Al-Janabi AS. Promising bio-active complexes of platinum (II) and palladium (II) derived from heterocyclic thiourea: synthesis, characterization, DFT, molecular docking, and anti-cancer studies. J Mol Struct. 2022;1252:132198.
18. Alsehli M, Aljuhani A, Ihmaid SK, El-Messery SM, Othman DI, El-Sayed AAA, Aouad MR. Design and synthesis of benzene homologues tethered with 1, 2, 4-triazole and 1, 3, 4-thiadiazole motifs revealing dual MCF-7/HepG2 cytotoxic activity with prominent selectivity via histone demethylase LSD1 inhibitory effect. Int J Mol Sci. 2022;23:8796.
19. Zhang N, Wang J, Sheng A, Huang S, Tang Y, Ma S, Hong G. Emodin Inhibits the proliferation of MCF-7 human breast cancer cells through activation of the aryl hydrocarbon receptor (AhR). Front Pharmacol. 2021;11:622046.
20. Emam MA, Khattab HI, Hegazy MG. Assessment of anticancer activity of Pulicaria undulata on hepatocellular carcinoma HepG-2 cell line. Tumor Biol. 2019;41:1010428319880080.
21. Huang TE, Deng YN, Hsu JL, Leu WJ, Marchesi E, Capobianco ML, Hsu LC. Evaluation of the anticancer activity of a bile acid-dihydroartemisinin hybrid ursodeoxycholic-dihydroartemisinin in hepatocellular carcinoma cells. Front Pharmacol. 2020;11:599067.
22. Zhou RS, Wang XW, Sun QF, Ye ZJ, Liu JW, Zhou DH, Tang Y. Anticancer effects of emodin on HepG2 cell: evidence from bioinformatic analysis. BioMed Res Int. 2019. https://doi.org/10.1155/2019/3065818.
23. Razak NA, Abu N, Ho WY, Zamberi NR, Tan SW, Alitheen NB. Yeap SK Cytotoxicity of eupatorin in MCF-7 and MDA-MB-231 human breast cancer cells via cell cycle arrest, anti-angiogenesis, and induction of apoptosis. Sci Rep. 2019;9:1–12.
24. Li J, Wang X, Shao Y, Lu X, Chen B. A novel exploration of a combination of gambogic acid with TiO_2 nanofibers: the photodynamic effect for HepG2 cell proliferation. Materials. 2014;7:6865–78.
25. Dang Y, Guan J. Nanoparticle-based drug delivery systems for cancer therapy. Smart Mater Med. 2020;1:10–9.
26. Adepu S, Ramakrishna S. Controlled drug delivery systems: current status and future directions. Molecules. 2021;26:5905.
27. Wilczewska AZ, Niemirowicz K, Markiewicz KH, Car H. Nanoparticles as drug delivery systems. Pharmacol Rep. 2012;64:1020–37.
28. Santhosh SB, Dutta D, Nath LK, Nanjan MJ, Chandrasekar MJN. Targeting ovarian solid tumors by pH triggered thermosensitive peptide-doxorubicin conjugate. J Drug Deliv Sci Technol. 2020;59:101856.
29. Garshasbi H, Salehi S, Naghib SM, Ghorbanzadeh S, Zhang W. Stimuli-responsive injectable chitosan-based hydrogels for controlled drug delivery systems. Front Bioeng Biotechnol. 2023;10:1126774.
30. Yang C, Wu X, Liu J, Ding B. Stimuli-responsive nucleic acid nanostructures for efficient drug delivery. Nanoscale. 2022;14:17862–70.
31. Rust T, Jung D, Langer K, Kuckling D. Stimuli-accelerated polymeric drug delivery systems. Polym Int. 2023;72:5–19.
32. Mohanan S, Guan X, Liang M, Karakoti A, Vinu A. Stimuli-responsive silica silanol conjugates: strategic nanoarchitectonics in targeted drug delivery. Small. 2023:e2301113. https://doi.org/10.1002/smll.20230 1113.
33. Das BC, Chokkalingam P, Masilamani P, Shukla S, Das S. Stimuli-responsive boron-based materials in drug delivery. Int J Mol Sci. 2023;24:2757.
34. Ahmad G, El Sadda R, Botchkina G, Ojima I, Egan J, Amiji M. Nanoemulsion formulation of a novel taxoid DHA-SBT-1214 inhibits prostate cancer stem cell-induced tumor growth. Cancer Lett. 2017;406:71–80.
35. Gavas S, Quazi S, Karpiński TM. Nanoparticles for cancer therapy: current progress and challenges. Nanoscale Res Lett. 2021;16:173.
36. Varlamova EG, Goltyaev MV, Simakin AV, Gudkov SV, Turovsky EA. Comparative analysis of the cytotoxic effect of a complex of selenium

El Sadda *et al. BMC Chemistry*   (2024) 18:35

Page 16 of 17

nanoparticles doped with sorafenib, "naked" selenium nanoparticles, and sorafenib on human hepatocyte carcinoma HepG2 cells. Int J Mol Sci. 2022;23:6641.

37. Matsushita T, Ketayama M, Kamihata KI, Funatsu K. Anchorage-dependent mammalian cell culture using polyurethane foam as a new substratum for cell attachment. Appl Microbiol Biotechnol. 1990;33:287–90.

38. Mattu C, Silvestri A, Wang TR, Boffito M, Ranzato E, Cassino C, Ciardelli G. Surface-functionalized polyurethane nanoparticles for targeted cancer therapy. Polym Int. 2016;65:770–9.

39. Weyermann J, Lochmann D, Georgens C, Zimmer A. Albumin-protamine-oligonucleotide-nanoparticles as a new antisense delivery system. Part 2: Cellular uptake and effect. Eur J Pharm Biopharm. 2005;59:431–8.

40. Crisante F, Francolini I, Bellusci M, Martinelli A, D'ilario L, Piozzi A. Antibiotic delivery polyurethanes containing albumin and polyallylamine nanoparticles. Euro J Pharm Sci. 2009;36:555–64.

41. Mattu C, Boffito M, Sartori S, Ranzato E, Bernardi E, Sassi MP, Di Rienzo AM, Ciardelli G. Therapeutic nanoparticles from novel multiblock engineered polyesterurethanes. J Nanopart Res. 2012;14:1–13.

42. Gentile P, Bellucci D, Sola A, Mattu C, Cannillo V, Ciardelli G. Composite scaffolds for controlled drug release: role of the polyurethane nanoparticles on the physical properties and cell behaviour. J Mech Behav Biomed Mater. 2015;44:53–60.

43. Song N, Ding M, Pan Z, Li J, Zhou L, Tan H, Fu Q. Construction of targeting-clickable and tumor-cleavable polyurethane nanomicelles for multifunctional intracellular drug delivery. Biomacromol. 2013;14:4407–19.

44. Rocas P, Fernandez Y, Schwartz S, Abasolo I, Rocas J, Albericio F. Multifunctionalized polyurethane-polyurea nanoparticles: hydrophobically driven self-stratification at the o/w interface modulates encapsulation stability. J Mater Chem B. 2015;3:7604–13.

45. Switaj TL, Winter KJ, Christensen S. Diagnosis and management of foodborne illness. Am Fam Physician. 2015;92:358–65.

46. Vats A, Nigam P. Microbial infection pathogenesis and progression: A Critical Review. 2022. https://doi.org/10.5281/zenodo.7002860.

47. Na S, Kim JH, Rhee YK, Oh SW. Enhancing the antimicrobial activity of ginseng against *Bacillus cereus* and *Staphylococcus aureus* by heat treatment. Food Sci Biotechnol. 2018;27:203–10.

48. Navale V, Vamkudoth KR, Ajmera S, Dhuri V. *Aspergillus* derived mycotoxins in food and the environment: prevalence, detection, and toxicity. Toxicol Rep. 2021;8:1008–30.

49. Sheikh-Ali SI, Ahmad A, Mohd-Setapar SH, Zakaria ZA, Abdul-Talib N, Khamis AK, Hoque ME. The potential hazards of *Aspergillus* sp. in foods and feeds, and the role of biological treatment: a review. J Microbiol. 2017;52:807–18.

50. Kordzadeh-Kermani V, Schaffie M, Rafsanjani HH, Ranjbar M. A modified process for leaching of ilmenite and production of TiO_2 nanoparticles. Hydrometallurgy. 2020;198:105507.

51. Nguyen TH, Lee MS. A review on the recovery of titanium dioxide from ilmenite ores by direct leaching technologies. Miner Process Extr Metall Rev. 2019;40:231–47.

52. Yu S, Wai AM. Upgrading of Titanium Dioxide from Ilmenite Concentrate. ETSJ. 2020;2(2):245–49.

53. Moawed EA, Eissa MS, Al-Tantawy SA. Application of polyurethane foam/zinc oxide nanocomposite for antibacterial activity, detection, and removal of basic dyes from wastewater. Int J Environ Sci Technol. 2022. https://doi.org/10.1007/s13762-022-04428-w.

54. Abo-Ashour MF, Eldehna WM, Nocentini A, Bonardi A, Bua S, Ibrahim HS, Supuran CT. 3-Hydrazinoisatin-based benzenesulfonamides as novel carbonic anhydrase inhibitors endowed with anticancer activity: synthesis, in vitro biological evaluation and silico insights. Eur J Med Chem. 2019;184:111768.

55. Mosmann T. Rapid colorimetric assay for cellular growth and survival: application to proliferation and cytotoxicity assays. J Immunol Methods. 1983;65:55–63.

56. Balouiri M, Sadiki M, Ibnsouda SK. Methods for in vitro evaluating antimicrobial activity: a review. J Pharm Anal. 2019;6:71–9.

57. Wayne PA. Clinical and Laboratory Standards: methods for dilution antimicrobial susceptibility test for bacteria that grow aerobically. Clin Lab Stand. 2018.11th Ed.ISBN1-56238-836-3.

58. El-Fallal AA, Elfayoumy RA, El-Zahed MM. Antibacterial activity of bio-synthesized zinc oxide nanoparticles using Kombucha extract. SN Appl Sci. 2023;5:332.

59. Tabassi NR, Ghasemiyan R, Brandkam MR, Hosseinpour T, Abkenar SK, Nesaz FR, Salehzadeh A. Green synthesis of $TiFe_2O_4$@ Ag nanocomposite using spirulina platensis; characterization of their anticancer activity and evaluation of their effect on the expression of Bax, p53, and Bcl-2 genes in AGS cell line. J Cluster Sci. 2022;33:1601–11.

60. Cobos M, De-La-Pinta I, Quindós G, Fernández MJ, Fernández MD. Synthesis, physical, mechanical and antibacterial properties of nanocomposites based on poly (vinyl alcohol)/graphene oxide–silver nanoparticles. Polymers. 2020;12:723.

61. Hassan YA, Alfaifi MY, Shati AA, Elbehairi SEI, Elshaarawy RF, Kamal I. Co-delivery of anticancer drugs via poly (ionic crosslinked chitosan-palladium) nanocapsules: targeting more effective and sustainable cancer therapy. J Drug Deliv Sci Technol. 2022;69:103151.

62. El Sadda RR, Elshahawy ZR, Saad EA. Biochemical and pathophysiological improvements in rats with thioacetamide induced-hepatocellular carcinoma using aspirin plus vitamin C. BMC Cancer. 2023;23:175.

63. Payolla FB, Aleixo NA, Nogueira FAR, Massabni AC. In vitro studies of antitumor activity of vanadium complexes with orotic and glutamic acids. Rev Bras Cancerol. 2020;66:04649.

64. Abbas SY, Al-Harbi RA, El-Sharief MAS. Synthesis and anticancer activity of thiourea derivatives bearing a benzodioxole moiety with EGFR inhibitory activity, apoptosis assay and molecular docking study. Eur J Med Chem. 2020;198:112363.

65. Kavanagh A, Ramu S, Gong Y, Cooper MA, Blaskovich MA. Effects of microplate type and broth additives on microdilution MIC susceptibility assays. Antimicrob Agents Chemother. 2019;63:10–1128.

66. Fass RJ, Barnishan J. Minimal inhibitory concentrations of 34 antimicrobial agents for control strains *Escherichia coli* ATCC 25922 and *Pseudomonas aeruginosa* ATCC 27853. Antimicrob Agents Chemotherapy.1979;16:622–624.

67. El-Dein MMN, Baka ZA, Abou-Dobara MI, El-Sayed AK, El-Zahed MM. Extracellular biosynthesis, optimization, characterization and antimicrobial potential of *Escherichia coli* D8 silver nanoparticles. J Microbiol Biotechnol Food Sci. 2021;10:648–56.

68. Salama HM, Diab MA, El-Sonbati AZ, El-Mogazy MA, Eldesoky AM, Amin BH, El-Zahed MM. New potential Mn (II) mixed ligand complexes: synthesis, structural characterization, molecular docking, antibacterial activity and electrochemical studies. J Iran Chem Soc. 2023. https://doi.org/10.1007/s13738-023-02892-w.

69. Diab MA, El-Sayed AK, Abou-Dobara MI, Issa HR, El-Sonbati AZ. Polymer complexes: LXXX—characterization, DNA cleavage properties, antimicrobial activity and molecular docking studies of transition metal complexes of Schiff base. J Iran Chem Soc. 2023. https://doi.org/10.1007/s13738-023-02755-4.

70. El-Sonbati AZ, Diab MA, El-Sayed AK, Abou-Dobara MI, Gafer AA. Synthesis, characterization, molecular docking, DNA cleavage properties, and antimicrobial activity studies of mixed ligand complexes. Appl Organomet Chem. 2022;36:e6651.

71. Hossain MA, Park HC, Park SW, Park SC, Seo MG, Her M, Kang J. Synergism of the combination of traditional antibiotics and novel phenolic compounds against *Escherichia coli*. Pathogens. 2020;9:811.

72. Schleifer KH, Kandler O. Peptidoglycan types of bacterial cell walls and their taxonomic implications. Bacteriol Rev. 1972;36:407–77.

73. Rohde M. The Gram-positive bacterial cell wall. Microbiol Spectr. 2019;7:7–3.

74. Venkatasubbu GD, Baskar R, Anusuya T, Seshan CA, Chelliah R. Toxicity mechanism of titanium dioxide and zinc oxide nanoparticles against food pathogens. Colloids Surf, B. 2016;148:600–6.

75. Hou Y, Zhu S, Chen Y, Yu M, Liu Y, Li M. Evaluation of antibacterial activity of thiourea derivative TD4 against methicillin-resistant *Staphylococcus aureus* via destroying the NAD^+/NADH homeostasis. Molecules. 2023;28:3219.

76. Marzi M, Pourshamsian K, Hatamjafari F, Shiroudi A, Oliaey AR. Synthesis of new N-Benzoyl-N'-triazine thiourea derivatives and their antibacterial activity. Russ J Bioorg Chem. 2019;45:391–7.

77. Son JK, Zhao LX, Basnet A, Thapa P, Karki R, Na Y, Lee ES. Synthesis of 2, 6-diaryl-substituted pyridines and their antitumor activities. Eur J Med Chem. 2008;43:675–82.

78. Anbumani D, Vizhi Dhandapani K, Manoharan J, Babujanarthanam R, Bashir AKH, Muthusamy K, Kanimozhi K. Green synthesis and antimicrobial efficacy of titanium dioxide nanoparticles using Luffa acutangula leaf extract. J King Saud Univ Sci. 2022;34:101896.

79. Abdulazeem L, Al-Amiedi BH, Alrubaei HA, Al-Mawlah YH. Titanium dioxide nanoparticles as antibacterial agents against some pathogenic bacteria. Drug Invent Today. 2019;12:963–7.

80. Mahdy SA, Mohammed WH, Emad H, Kareem HA, Shamel R, Mahdi S. The antibacterial activity of TiO_2 nanoparticles. J Univ Babylon. 2017;25:955–61.

81. Younis AB, Milosavljevic V, Fialova T, Smerkova K, Michalkova H, Svec P, Dolezelikova K. Synthesis and characterization of TiO_2 nanoparticles combined with geraniol and their synergistic antibacterial activity. BMC Microbiol. 2023;23:207.

82. Costa EP, Roccamante M, Amorim CC, Oller I, Pérez JAS, Malato S. New trend on open solar photoreactors to treat micropollutants by photo-Fenton at circumneutral pH: Increasing optical pathway. Chem Eng J. 2020;385:123982.

83. El-Zahed MM, El-Sonbati MA, Farhat AA, Moawed EA, Kiwaan HA. Application of thiourea polyurethane@ copper sulfide composite for antibacterial potential. Egypt J Chem. 2023;66:31–6.

84. Mohamed NA, Al-mehbad NY. Novel terephthaloyl thiourea cross-linked chitosan hydrogels as antibacterial and antifungal agents. Int J Biol Macromol. 2013;57:111–7.

Publisher's Note